# The influence of nanoscale grooved substrates on osteoblast behavior and extracellular matrix deposition

Edwin Lamers [a], X. Frank Walboomers [a], Maciej Domanski [b], Joost te Riet [c,d], Falco C.M.J.M. van Delft [e], Regina Luttge [b], Louis A.J.A. Winnubst [b], Han J.G.E. Gardeniers [b], John A. Jansen [a,*]

[a] Department of Biomaterials, Radboud University Nijmegen Medical Centre, P.O. Box 9101, 6500 HB, Nijmegen, The Netherlands
[b] MESA+ Institute for Nanotechnology, University of Twente, P.O. Box 217, 7500 AE, Enschede, The Netherlands Enschede, The Netherlands
[c] Department of Scanning Probe Microscopy, Institute for Molecules and Materials, Radboud University, Nijmegen, The Netherlands
[d] Department of Tumor Immunology, Nijmegen Centre for Molecular Life Sciences, Radboud University Nijmegen Medical Centre, P.O. Box 9101, 6500 HB Nijmegen, The Netherlands
[e] Philips Research (MiPlaza), 5656 AE Eindhoven, The Netherlands

## ARTICLE INFO

## ABSTRACT

To fight bone diseases characterized by poor bone quality like osteoporosis and osteoarthritis, as well as in reconstructive surgery, there is a need for a new generation of implantable biomaterials. It is envisioned that implant surfaces can be improved by mimicking the natural extracellular matrix of bone tissue, which is highly a organized nano-composite. In this study we aimed to get a better understanding of osteoblast response to nanometric grooved substrates varying in height, width and spacing. A throughput screening biochip was created using electron beam lithography. Subsequently, uniform large-scale nanogrooved substrates were created using laser interference lithography and reactive ion etching. Results showed that osteoblasts were responsive to nanopatterns down to 75 nm in width and 33 nm in depth. SEM and TEM studies showed that an osteoblast-driven calcium phosphate (CaP) mineralization was observed to follow the surface pattern dimensions. Strikingly, aligned mineralization was found on even smaller nanopatterns of 50 nm in width and 17 nm in depth. A single cell based approach for real time PCR demonstrated that osteoblast-specific gene expression was increased on nanopatterns relative to a smooth control. The results indicate that nanogrooves can be a very promising tool to direct the bone response at the interface between an implant and the bone tissue.

© 2010 Elsevier Ltd. All rights reserved.

## 1. Introduction

The use of implants has become a common treatment for end stage destructive joint diseases like osteoporosis, osteoarthritis and bone tumors. These bone diseases are characterized by poor bone quality, decreased bone formation or increased bone resorption. Current therapy includes the replacement of damaged tissue by the installation of an implant. To increase the lifespan of implants in these compromised patients, there is a need for a new generation of implantable biomaterials, for which it is supposed that improvement of initial bone tissue response should lead to long-term implant stability.[1] This initial response depends on several factors, but most important are the interface interactions between bone tissue and the biomaterial surface. Key parameters are surface wettability and surface topography.[2] Cells are known to be very sensitive to the

surface topographical environment and recognize surface topographical alterations, which subsequently can induce changes in the cytoskeleton, cell shape and differentiation.[3] Besides this cellular effect, surface nanostructure can serve as a template to control the initiation and growth of apatite crystals, the major building block of bone tissue.[4] In this context it is envisioned that one approach to improve interface interactions between implants and the surrounding bone tissue is by mimicking the natural extracellular matrix (ECM) of bone tissue in order to stimulate osteoblast adhesion, proliferation and differentiation. The natural bone ECM is a highly organized nanocomposite, consisting of molecules like collagen type-1 and hydroxyapatite[5,6]. Collagen type-I forms fibrils with an interfibrillar spacing of 68 nm and 35 nm depth. The hydroxyapatite crystals are embedded in these fibrils [6] and have an average size of $50 \times 25 \times 4$ nm$^3$. The bone surface has an average roughness value ($R_a$) of 32 nm.[7] Many groups have already verified the effect of mimicking the bone surface nanoroughness using various biomaterials [7–18] and showed a beneficial effect of nanoroughness on osteoblast proliferation.[8,9,13,14] However in all these

studies, nanometric surface structures were formed by random processes like self-organization via polymer demixing, colloidal lithography, acid etching or grinding.[11,12,17] The response of osteoblasts to ordered textures has also been reported, but merely on a micrometer (i.e. $>1\,\mu m$) or sub-micrometer topography (i.e. $1\,\mu m > 100\,nm$).[19–21] It is shown that cells are especially responsive to groove/ridge patterns and on such surfaces aligned as well as migrated along the groove direction. Also ECM formation [22] and mineral deposition has been shown to be promoted along such sub-micrometer grooves.[21] However, so far most studies focused on the cell response to grooves with only one dimension (either depth or width) in the nanometer scale (i.e. 1–100 nm), while leaving the other dimension always at micron or just submicron-scale, i.e. considerably larger than the natural bone ECM [20,21,23,24].

In this paper, we report on the response of osteoblast-like cells to grooved substrates nanometric in all dimensions. Several aspects of the cellular response were studied, i.e., (1) adjustment of the shape of osteoblasts and the position of focal adhesions, (2) the interface between osteoblast-like cells and substrates, and (3) gene expression profiles.

## 2. Materials and methods

### 2.1. Substrates

A silicon biochip containing 50 different nanometric patterns was generated using electron beam lithography (EBL) as described by Loesberg et al. [25] employing Hydrogen Silsesquioxane resist, as described by van Delft et al. [26,27] The field patterns consisted of squares of $500 \times 500\,\mu m$ containing patterns with nanogroove-to-ridge ratios of 1:1, 1:3 and 3:1. As a control for cellular orientation, silicon substrates with microgrooves (depth of $0.25\,\mu m$ and a pitch of $2\,\mu m$; [28]), as well as smooth substrates were used. All silicon substrates were used as templates for the production of polystyrene (PS; Acros, Geel, Belgium) replicates for cell culture [28].

### 2.2. Large scale uniform nanogrooved substrates created with laser interference lithography

After screening of the biochip, also large scale, uniformly nanogrooved silicon wafers were created using laser interference lithography (LIL). A setup was used based on the Lloyd's interferometer, where a regular pattern was produced by interference of an incident laser beam and a mirror reflected beam.[29] The period of the interference pattern, and thus of the grating recorded in the resist layer on the substrate, is given by the equation: $P = \lambda/(2\sin q)$ where the period ($P$) is determined by the wavelength ($\lambda$) of the beam source and the angle ($q$) at which two coherent beams are interfering. With a 266 nm light source, periods of 150 nm up to 1000 nm were produced.[30] An optimized antireflective photoresist layer [30] was spin coated on a silicon wafer. After illumination and development of the resist layer, the grating was transferred to the substrate by a reactive ion etching process using a Plasmatherm 790 system (Unaxis, Utrecht, The Netherlands). An optimized method of reactive ion etching using parameters giving anisotropic etch profiles in nanoscale was used. $SF_6:O_2$ (instead of $CHF_3:O_2$) plasma chemistry gave well defined structures transferred on silicon. Using this setup, highly regular patterns were produced over areas of about $2 \times 2\,cm^2$.

### 2.3. Polystyrene replicas

For the reproduction of the PS replicas, 0.5 g PS dissolved in 3 mL chloroform was casted onto a 3″ silicon wafer and the chloroform was evaporated. PS rings (2.0 cm $\varnothing$) were glued to substrates using a small amount of casting solution to create cell culture dishes. Substrates received a radiofrequency glow-discharge (RFGD; Harrick, Ossining, USA) treatment for 5 min at $10^{-2}$ mbar for sterilization and to improve wettability.

### 2.4. Atomic force microscopy (AFM)

Surface topography was quantitatively evaluated using a Dimension atomic force microscope (AFM; Dimension 3100, Veeco, Santa Barbara, CA). Tapping in ambient air was performed with 118 μm long silicon cantilevers (NW-AR5T-NCHR, NanoWorld AG, Wetzlar, Germany) with average nominal resonant frequencies of 317 kHz and average nominal spring constants of 30 N/m. This type of AFM probe has a high aspect ratio (7:1) portion of the tip with a nominal length of $>2\,\mu m$ and a half-cone angle of $<5°$. Nominal radius of curvature of the AFM probe tip was less than 10 nm. The probes are especially suited to characterize the manufactured nanogrooves.

Height images of each field/sample were captured in ambient air at 50% humidity at a tapping frequency of 266.4 kHz. The analysed field was scanned at a scan rate of 0.5 Hz and 512 scanning lines. Nanoscope imaging software (version 6.13r1, Veeco) was used to analyse the resulting images. Surface roughness (root mean squared (RMS), nm) and depth (nm) were obtained and averaged for three random fields per substrate.

### 2.5. Cell culture

Osteoblast-like cells were obtained as described before [31]. Briefly, femurs of 40–43 day old male Wistar WU rats (local approval number DEC 2004156). The femurs were washed three times in alpha Minimal Essential Medium (αMEM; Gibco, Invitrogen Corp., Paisley, Scotland) with 0.5 mg/mL gentamycin and 3 μg/mL fungizone. The epiphyses were removed and the diaphyses were flushed out cell culture medium containing 10% fetal calf serum (Gibco), 50 μg/ mL ascorbic acid (Sigma–Aldrych, Zwijndrecht, the Netherlands), 10 mM Na-β-glycerophosphate (Sigma), $10^{-8}$ M dexametasone (Sigma) and 50 μg/mL gentamycin (Gibco).

After one day medium was refreshed to remove non-adherent cells. After 7 days of primary culture, cells were detached with trypsin/EDTA (0.25% w/v trypsin/0.02% EDTA) and seeded onto the substrates at $10^4$ cells/cm$^2$.

### 2.6. Cellular orientation

At 24 h, cells were washed in PBS and fixed for 10 min in 3% formaldehyde (PFA; Sigma–Aldrych) and 0.02% glutaraldehyde (Acros) in PBS. Cells were permeabilized in 1% Triton X100 (Koch, Colnbrook, England) in PBS for 5 min and subsequently incubated with PBS containing 5% BSA (Sigma) for 30 min to block aspecific epitopes. Actin filaments of cells were fluorescently stained with Alexa-fluor 568 conjugated phalloidin (1:200 Molecular probes, Invitrogen Corp., Paisley, Scotland) diluted in PBS containing 1% BSA and 0.1% Tween-20 (Merck, Schuchardt, Germany). The specimens were examined using an Olympus FV1000 confocal laser scanning microscope (CLSM, Olympus, Center Valley, USA).

Orientation of osteoblast-like cells on grooved substrates was examined by taking photographs of cells and determining the angle relative to the line direction. The images were analysed with ImageJ software (Image J, La Jolla, USA). Inclusion criteria for cells were: the cell was not in contact with other cells and the cell was not in contact with the image perimeter. Statistical analysis was performed using SPSS for Windows (SPSS14.0, Chicago, USA).

## 2.7. Immunofluorescence staining

After 24 h, osteoblast-like cells were washed 3 times in PBS and fixed for 10 min in 3% PFA and 0.02% glutaraldehyde in PBS and permeabilized in 1% Triton X100 in PBS for 5 min. Cells were then incubated in PBS containing 5% BSA for 30 min to block aspecific epitopes. α-Vinculin labelling was performed overnight with mouse monoclonal primary antibodies (1:500; Sigma) in PBS containing 1% BSA and 0.1% Tween-20. This incubation step was followed by incubation with goat anti-mouse secondary antibody Alexa-fluor 488 conjugated IgG (1:200; Molecular Probes, Invitrogen), Alexa-fluor 568 conjugated phalloidin for F-actin fluorescence (1:200; Molecular probes) and DAPI staining for nucleic UV-visualization (1:2500) diluted in PBS containing 1% BSA and 0.1% Tween-20 for 2 h at room temperature. Finally, the specimens were examined with an Olympus FV1000 CLSM.

## 2.8. Transmission electron microscopy (TEM)

Osteoblast-like cells were cultured for 12 and 16 days and subsequently washed in PBS, fixed in 2% glutaraldehyde in 0.1 M sodium-cacodylate for 5 min and washed in 0.1 M sodium-cacodylate. Subsequently cells were post-fixed in 1% $OsO_4$ for 60 min and dehydrated in a graded series of ethanol (5 min in 70%, 80%, 90%, 96%, 100% ethanol and finally 100% filtered ethanol). The patterned areas were then cut into pieces and embedded in epoxy resin (Electron Microscopy Sciences, Hatfield, USA). The specimens were first incubated overnight in a mixture of 1:1 Epoxy resin:EtOH 100%, washed three times in pure epoxy resin and then incubated overnight in pure epoxy resin. The epoxy resin was polymerized at 65 °C. After polymerization ultrathin sections of approximately 130 nm thickness were cut for TEM analysis using a diamond knife (Diatome) and collected on 100 mesh grids (Electron microscopy sciences, Hatfield, USA). After drying, sections were stained in uranyl acetate for 30 min and subsequently in lead citrate for 10 min. Sections were examined with a JEOL TEM 1010 (Nieuw Vennep, the Netherlands). The electron dense areas observed with TEM, were further analyzed using EDX-TEM analysis (FEI, Eindhoven, The Netherlands).

## 2.9. Scanning electron microscopy (SEM)

At 3, 8 and 16 days, cells were washed in PBS, fixed for 5 min in 2% glutaraldehyde in 0.1 M sodium-cacodylate and washed for 5 min in 0.1 M sodium-cacodylate. Fixed cells were dehydrated in a graded series of ethanol (5 min in 70%, 80%, 90%, 96%, 100% ethanol and finally 100% water free ethanol) and dried to air in tetramethylsilane. The specimens were sputter-coated with gold (10 nm) and examined with a Jeol 6310 SEM.

## 2.10. RNA isolation and reverse transcriptase PCR

Cells were cultured for 12 h, 48 h and 5days, washed 3x in PBS and subsequently excised from nanogrooved substrates of 1000 nm, 300 nm and 150 nm groove pitch. Since cells were seeded at such a low density, conventional reverse transcriptase and QPCR was replaced by a single-cell based approach as described by Shieh et al. [32] mRNA isolation was performed using the Absolutely RNA® Nanoprep kit (Stratagene, La Jolla, USA) according to manufacturer's protocol. Briefly, the cells were lysed in 100 μL of lysis buffer containing 0.7 μL of β-mercaptoethanol. Subsequently 100 μL EtOH 70% was added, thoroughly mixed and transferred into an RNA-binding nano-spin cup. The sample was centrifuged at 12,000×g for 60 s, the filtrate was discarded and 300 μL of low-salt wash buffer was added. The sample was centrifuged and the filtrate

was removed. 15 μL of DNase-solution (2.5 μL RNase-Free DNase-I mixed with 12,5 μL DNase digestion buffer) was added to the sample and incubated for 15 min at 37 °C. 300 μL of high-salt wash buffer was added to and subsequently centrifuged at 12,000×g for 1 min. The filtrate was discarded, 300 μL low-salt wash buffer was added to the spin-cup and centrifuged. 8 μL of Elution buffer was added to the sample and incubated for 2 min at room temperature. The sample was collected by centrifugation at 12,000×g for 5 min.

After obtaining the mRNA, a first strand reverse transcriptase PCR was performed using the Superscript™ III First-strand Synthesis System for RT-PCR (Invitrogen) according to manufacturers protocol. The collected 8 μL of mRNA was incubated with 1 μL of dNTPs (1 mM end concentration), 0.5 μL random hexamers and 0.5 μL oligo (dT)$_{20}$ primers (both 0.5 μM end concentration) for 5 min at 65 °C to anneal the primers to the mRNA. The following components were subsequently added: 2 μL 10× reaction buffer, 4 μL 25 mM $MgCl_2$, 2 μL 0.1 M DTT, 1 μL RNaseOUT (40 U/μL) and 1 μL superscript III RT (200 U/μL). The reaction mix was incubated for 10 min at 25 °C for further primer annealing, 50 min at 50 °C for reverse transcription and 5 min at 85 °C to terminate the reaction. Then 1 μL RNase H was added to the tube and incubated for 20 min at 37 °C for RNA digestion. This solution was stored at −20 °C until further use.

## 2.11. Real time PCR

The cDNA will then be amplified and specific gene expression is quantified in a real-time PCR. For this reaction, 12.5 μL master mix, 2 μL DNA, 3 μL primer mix (1.5 μL forward primer and 1.5 μL reverse primer are mixed) and 7.5 μL DEPC. Subsequently the PCR is performed in a Real-Time PCR reaction apparatus with the desired temperatures. The used primers were from β1-integrin, β3-integrin, collagen type-I, alkaline phosphatase (ALP), osteocalcin (OCN), osteopontin (OPN) and β-actin (sequences are given in Table 1). The expression of the tested genes was calculated via the $2^{-\Delta\Delta Ct}$ method [33] relative to smooth controls. Statistical analysis was performed using SPSS for Windows (SPSS 14).

# 3. Results

## 3.1. Substrates

Biochip templates and PS replicates were routinely checked by atomic force microscopy (AFM) (Fig. 1a, b) and scanning electron

**Table 1**
Overview of the sequences of the used primers.

| Primer | Sequence |
| --- | --- |
| Col-1 | F5′-AACCCGAGGTATGCTTGATCT-3′ |
| | R5′-CCAGTTCTTCATTGCATTGC-3′ |
| ALP | F5′-GGGACTGGTACTCGGATAACGA-3′ |
| | R5′-CTGATATGCGATGTCCTTGCA-3′ |
| Cbfa1 | F5′-GCCACACTTTCCACACTCTC-3′ |
| | R5′-CACTTCTGCTTCTTCGTTCTC-3′ |
| OCN | F5′-CGGCCCTGAGTCTGACAAA-3′ |
| | R5′-GCCGGAGTCTGTTCACTACCTT-3′ |
| BSP | F5′-TCCTCCTCTGAAACGGTTTCC-3′ |
| | R5′-GGAACTATCGCCGTCTCCATT-3′ |
| β-Actin | F5′-TTCAACACCCCAGCCATGT-3′ |
| | R5′-TGTGGTACGACCAGAGGCATAC-3′ |
| Int α1 | F5′-AGCTGGACATAGTCATCGTC-3′ |
| | R5′-AGTTGTCATGCGATTCTCCG-3′ |
| Int β1 | F5′-AATGTTTCAGTGCAGAGCC-3′ |
| | R5′-TTGGGATGATGTCGGGAC-3′ |
| GapdH | F5′-TCCTGCACCACCAACTGCTT-3′ |
| | R5′-GAGGGGCCATCCACAGTCTT-3′ |

**a**



**b**
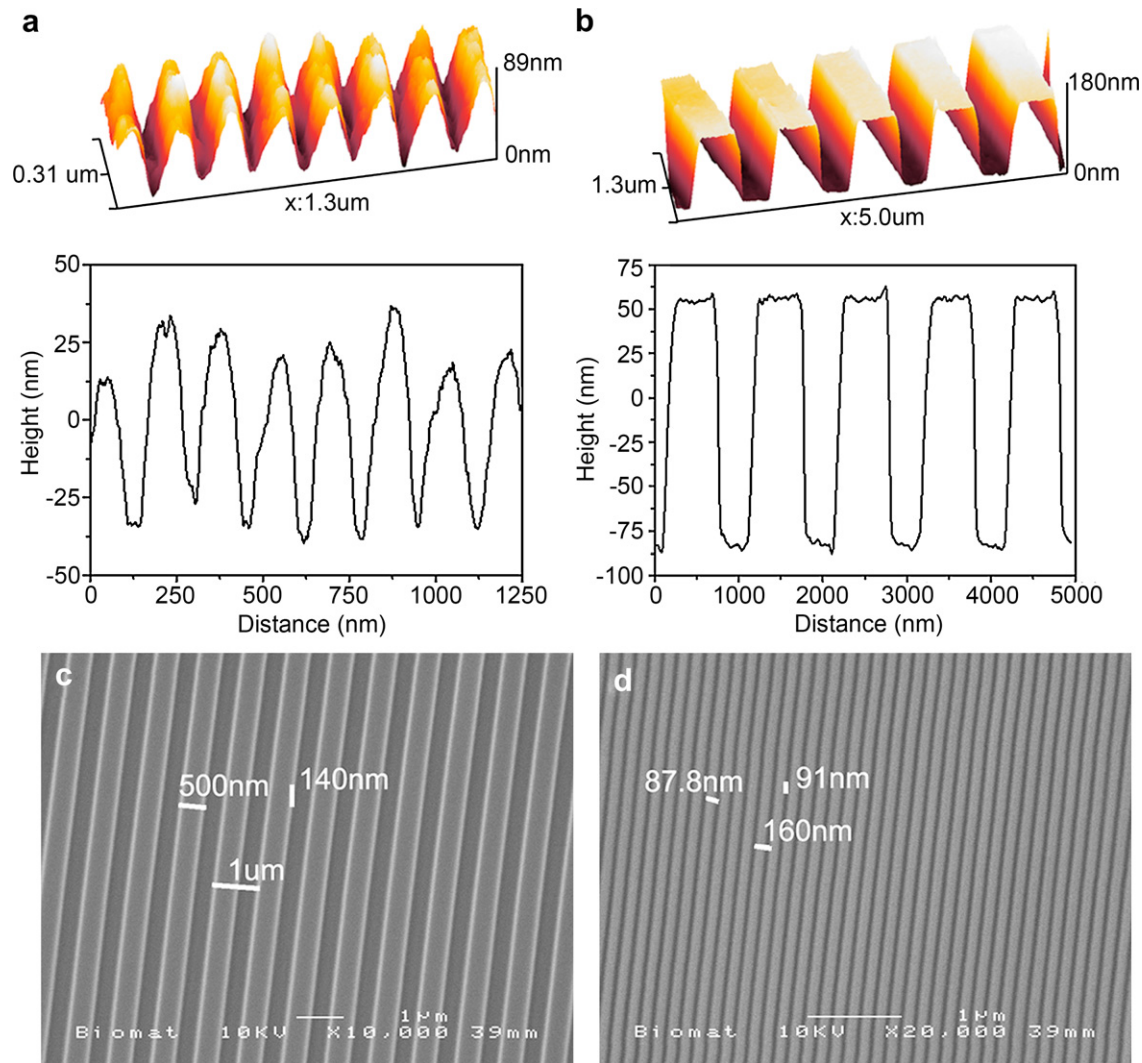


**Fig. 1.** Three-dimensional (3D) AFM topography image and height profile of silicon wafers with groove dimensions of (a) a width of 300 nm and a depth of 158 nm. 3D AFM topography image and height profile of a PS-substrate with (b) a width of 500 nm and a depth of 153 nm. SEM graphs of PS-substrates with a width of (c) 500 nm and (d) 80 nm.

microscopy (SEM) (Fig. 1c, d). The dimensions are summarized in Table 2.

Similar large-scale nanotextures of $2 \times 2\,cm^2$ were produced using laser interference lithography (LIL) followed by reactive ion etching (RIE). This technique was applied to facilitate both qualitative and quantitative *in vitro* studies. The LIL-derived silicon substrates and the PS replicates were analyzed using AFM and SEM (PS replicates are shown in Fig. 2 and a list of dimensions is given in Table 2).

### 3.2. Cellular orientation

The studied groove/ridge patterns had an evident effect on osteoblast morphology, and were found to induce alignment of the osteoblast cell shape and internal F-actin filaments (Fig. 3a). On textures with sizes equivalent to the natural bone ECM (i.e. a groove width of 150–75 nm and depth down to 33 nm; region between red lines in Fig. 3c) a clear interaction between the grooves and cells resulting in alignment was found, while on dimensions with a width of 50 nm and a 17 nm depth or smaller (Fig. 3b) cells did spread randomly. An analysis of the alignment is shown quantitatively in a Box–Whisker plot (Fig. 3c). Alignment of

**Table 2**
Feature dimensions of topographically patterned substrata.

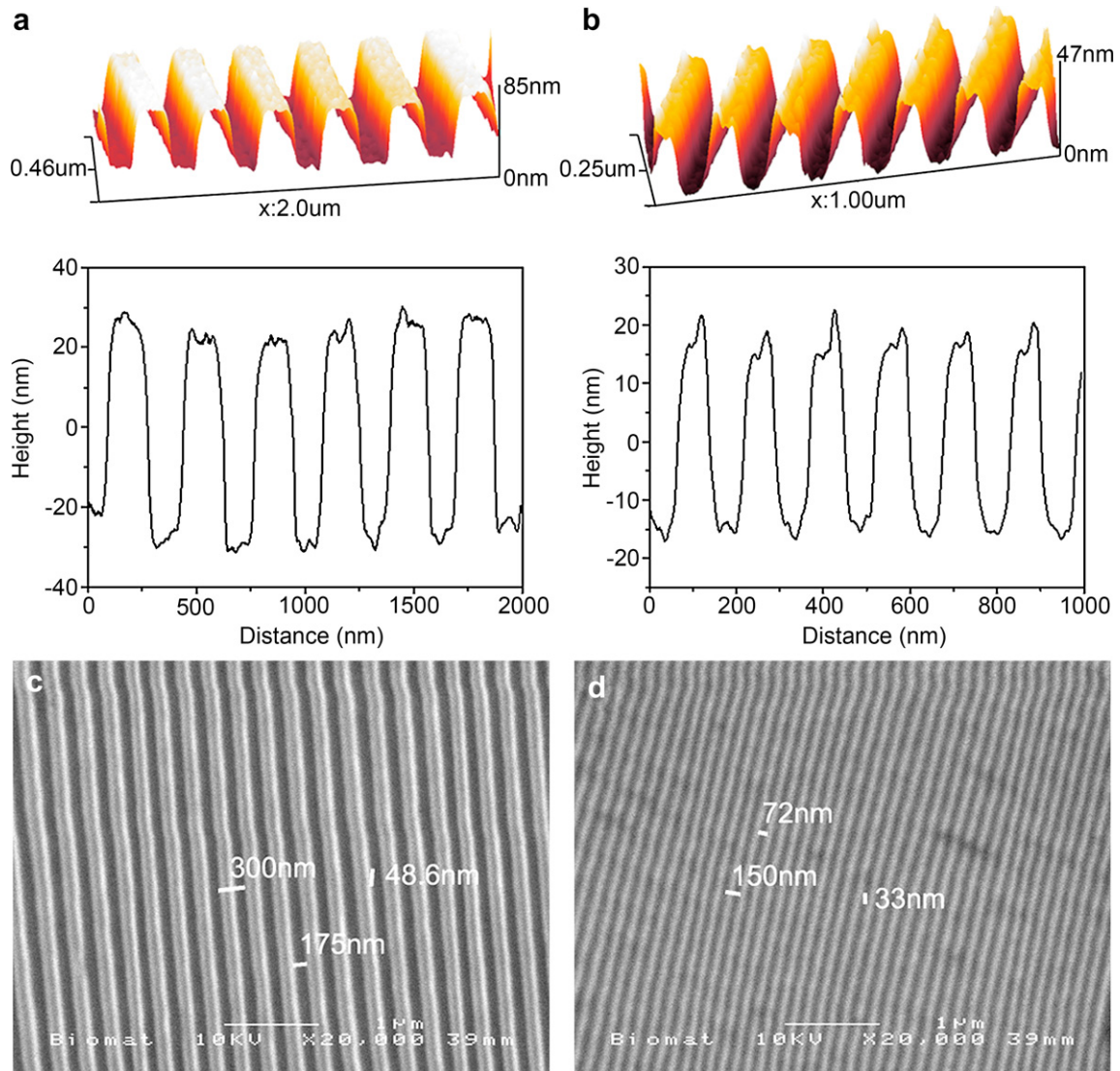| E-beam derived biochip | | |
|---|---|---|
| Pitch (nm) | Depth (nm + SE) | Roughness (nm ± SE) |
| 1000 | 153.3 ± 2.7 | 69.1 ± 1.0 |
| 600 | 158.0 ± 3.2 | 64.4 ± 0.7 |
| 400 | 149.2 ± 1.2 | 53.9 ± 1.8 |
| 300 | 119.9 ± 2.6 | 36.7 ± 1.3 |
| 200 | 77.4 ± 4.1 | 22.0 ± 0.5 |
| 160 | 51.9 ± 3.4 | 15.3 ± 0.3 |
| 100 | 17.2 ± 3.5 | 9.2 ± 0.7 |
| 80 | 15.3 ± 1.9 | 8.7 ± 0.9 |
| 60 | 11.6 ± 1.1 | 8.3 ± 0.1 |
| 40 | 10.9 ± 1.1 | 6.6 ± 0.4 |
| 2000 | 353.9 ± 8.2 | 163.3 ± 10.5 |
| *LIL-derived substrates* | | |
| 1000 | 158 ± 10 | |
| 600 | 122.3 ± 10 | |
| 300 | 48.6 ± 1.8 | 31 |
| 200 | 51.8 ± 2.7 | 27 |
| 150 | 32.7 ± 2.0 | 18 |

**Fig. 2.** 3D AFM topography image and height profiles of LIL-derived PS-substrates with a width of (a) 150 nm (49 nm depth) and (b) 75 nm (33 nm depth). SEM graphs of substrates with a width of (c) 150 nm and (d) 75 nm.

osteoblasts on the LIL-derived substrates was similar to the corresponding biochip dimensions (Fig. 3c, asterisks).

A trend analysis of deviation of osteoblast alignment from the average median of all data (10°, red line in Fig. 3c) in Fig. 3d showed that: (1) cells aligned to sub micrometer grooves, and (2) osteoblast alignment gradually decreased with decreasing groove widths ($p$-value $< 0.01$). This phenomenon was persistent down to a groove width of 75 nm and depth of 33 nm. Below this point cells did not morphologically recognize surface topography anymore. This dimension can therefore be considered a threshold point for morphological nanopattern recognition by osteoblasts.

### 3.3. Focal adhesions

It was observed that focal adhesions were mainly oriented to the groove direction on groove widths down to 150 nm (and 120 nm depth) (Fig. 4a, b), whereas focal adhesions were oriented randomly on surfaces with a groove width of less than 50 nm (and depth of 17 nm) (Fig. 4c). In agreement with cellular alignment, a decreasing groove pitch resulted in decreased focal adhesion alignment (Fig. 4b). Higher magnification imaging revealed that the aligned focal adhesions tended to reside on top of the ridges (Fig. 4d).

### 3.4. Transmission and scanning electron microscopy

TEM images demonstrated that cells descended into grooves (Fig. 5b). The electron dense material deposited in between the grooves at the interface between cells and substrate surface (asterisks in Fig. 5a and c) was analyzed with energy dispersive X-ray analysis (EDX) and confirmed to be calcium and phosphorous (asterisks in Fig. 5, EDX in Fig. 5d). Additional electron dense areas (arrowheads in Fig. 5) as seen in TEM were found to consist of CaP and proteins (mainly collagen, arrows in Fig. 5) which corresponds to the formation of an extracellular mineralized matrix. Comparison of TEM sections at 12 and 16 days demonstrated that cell bodies in time are gradually driven away from the interface by a mineralized ECM; after 12 days of culture, osteoblasts resided inside the nanogrooves and only a small amount of CaP was shown to be deposited on the bottom of the grooves below the cells (Fig. 5b). However, after 16 days the interface consisted of a thick extracellular mineralized matrix layer produced by osteoblasts covering the ridges (Fig. 5c).

Further SEM analysis demonstrated that the CaP was deposited in an aligned mode after 8 days of culture (Fig. 6). Strikingly,
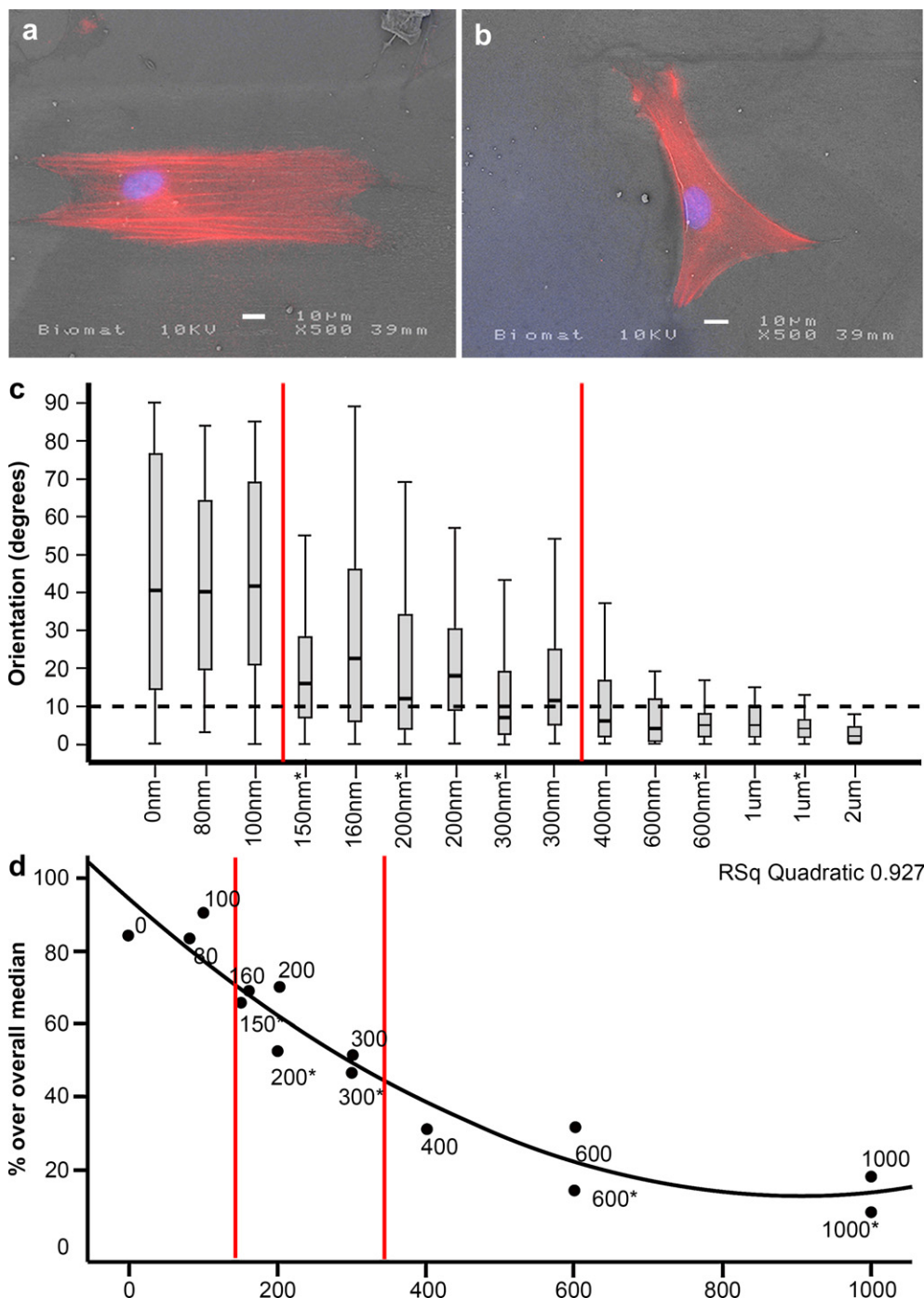
**Fig. 3.** Cell alignment of osteoblast-like cells to grooved substrates (overlay fluorescence and SEM image). Cells were stained for F-actin (red) and the nucleus (DAPI): (a) with a width of 150 nm (120 nm depth) and (b) a width of 50 nm (17 nm depth). (c) A Box-Whisker plot showing the cellular alignment to the nanogrooves (a median of 45° is random orientation). The median is marked in the box and the box-corners indicate the 25th to 75th percentiles. Note that cells start to align to nanopatterns from a minimal groove width of 75 nm (33 nm depth). The overall median orientation is 10° (dotted line). Asterisks represent the LIL-derived substrates. (d) Scatter plot of percentage of osteoblasts on the grooved patterns that are higher than the average median of 10°. The trend analysis demonstrates a groove dependent decrease of cellular orientation ($R^2$ of trendline is 0.93). The regions between the red lines are indicating the pattern sizes that are considered equivalent in size to the ECM.

whereas osteoblasts did not align to a groove width below 75 nm (and 33 nm depth), CaP deposition aligned even down to a groove width of 50 nm (and 17 nm depth) (Fig. 6b).

### 3.5. Real-time quantitative PCR analysis

The genes studied in the real-time quantitative (Q)PCR were coding for the four bone differentiation markers, (i.e. alkaline phosphatase (ALP), osteocalcin (OCN), bone sialoprotein (BSP) and the Cbfa1/Runx2 transcription factor (Cbfa1)), the major ECM protein collagen type-I (Col-I) as well as the α-1 and β-1 chains of the integrins, which are responsible for cell-substrate adhesion of cells. Relative gene expression was normalized to the household β-actin gene expression.

The expression of the tested genes was measured relative to smooth controls at three different time points ($t = 1$, 3 and 6 days)
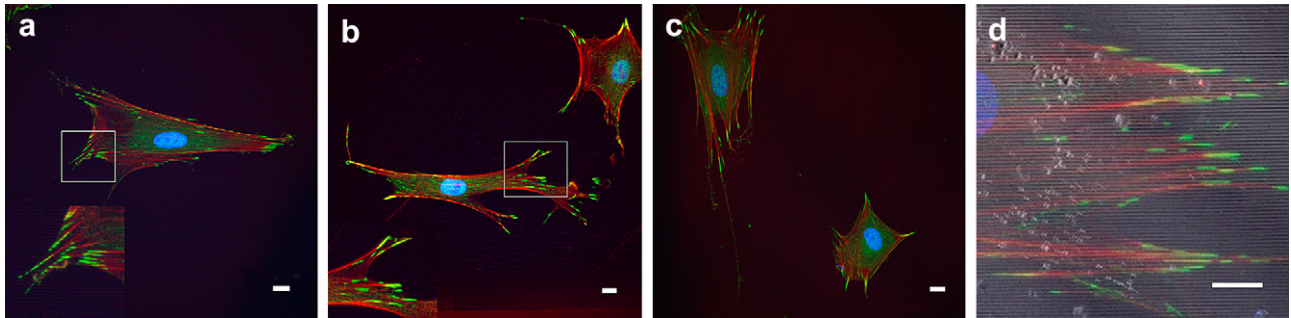
**Fig. 4.** Immunofluorescence micrograph of osteoblast-like cells cultured on nanogrooved substrates. Focal adhesions (α-vinculin, green) on a groove width of (a) 500 nm (153 nm depth) were mostly aligned with the groove direction, whereas alignment of focal adhesions to a groove width of (b) 150 nm (120 nm depth) had diminished and was random on a groove width of (c) 50 nm (17 nm depth). (d) An overlay of a fluorescent micrograph with a light micrograph. α-Vinculin staining on a width of 300 nm (158 nm depth) shows that focal adhesions mainly reside on top of the ridges. Green, vinculin; red, F-actin; blue, nuclei. Bars: 10 μm.

on three different groove pitches ($p = 1000$ nm, 3000 nm and 150 nm) for cells obtained from three different rats is shown in Table S1. The results demonstrated large differences in response to grooved relative to smooth substrates between the individual rats. Statistical analysis confirmed these differences (two-way Anova, $p < 0.05$, except for integrin-1β). However, data also demonstrated a clear pattern favoring the grooved substrates (Fig. 7a). In order to confirm this pattern, a ranking analysis was performed on the expression of the osteoblast specific markers (ALP, OCN, BSP, ColI and Cbfa1) between the four surfaces at three time points (Fig. 7b). The analysis confirmed that expression of osteoblast-specific genes

at day three and day six were increased on the grooved substrates compared to the smooth control (Friedman-test, $p < 0.05$). Moreover, the analysis indicated that a 500 nm groove width (158 nm depth) was more inductive for osteoblast differentiation than 150 and 75 nm widths (49 nm and 33 nm) respectively.

## 4. Discussion

The aim of this study was to understand the morphological and differentiation response of osteoblasts to nanogrooved substrates. In order to achieve this, osteoblast response to these grooves was
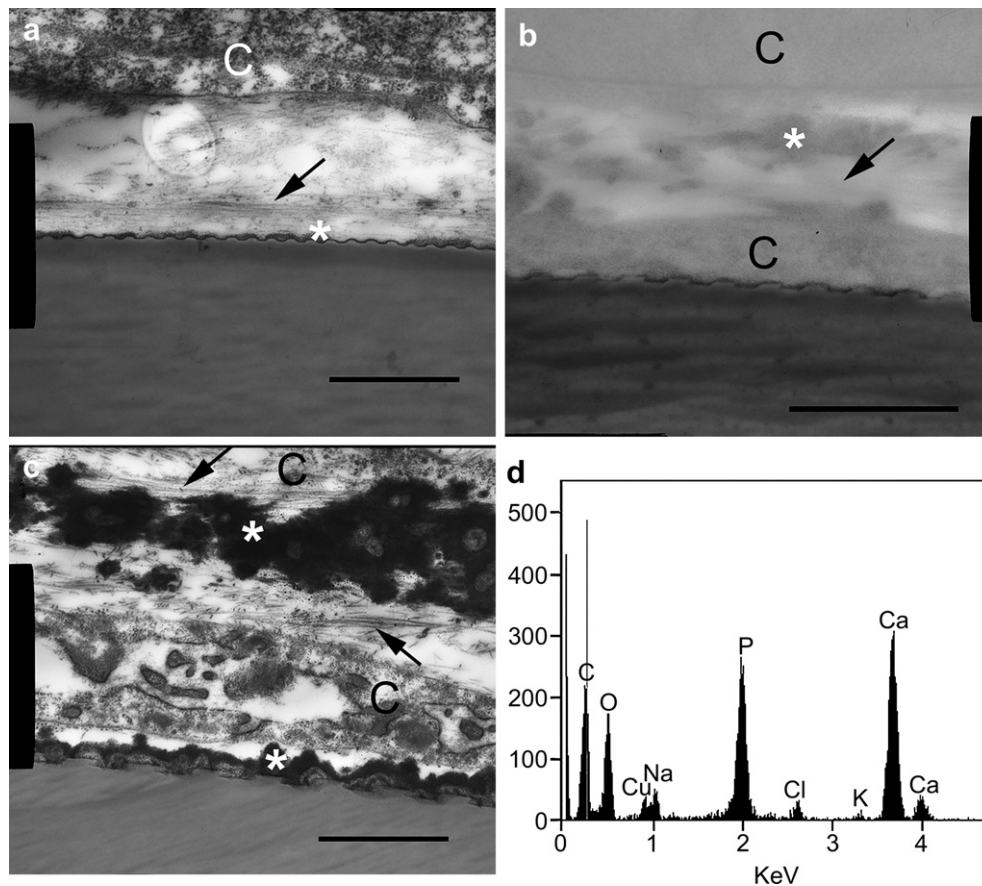


**Fig. 5.** TEM images of osteoblast-like cells cultured for 12 (a, b) or 16 days (c) on grooved substrates with groove widths of respectively a. 75 nm (33 nm depth), b. 150 nm (49 nm depth) and c. 300 nm (122 nm depth). An electron dense area is formed in the interface between cells and substrate (asterisks in (a) and (c)). In the intercellular regions a mineralized ECM is formed by the presence of CaP (arrowheads) and collagen-I (arrows). In b. is shown that osteoblast-like cell bodies descend into 150 nm wide grooves. (d). Elemental analysis in the interface (asterisks in (a), (c)) shows that the electron dense area is indeed mineralized ECM, i.e. rich in calcium and phosphate (phosphor). C: Cell body. Scale bars represent 1 μm.
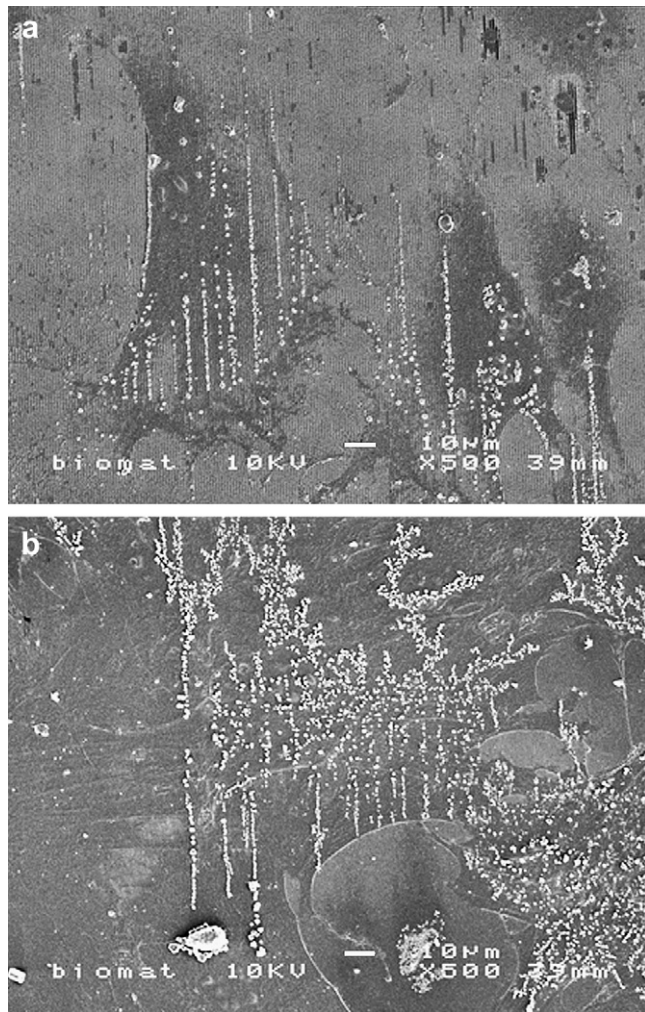
**Fig. 6.** SEM images of osteoblast-like cells cultured for 8 days on grooved substrates. Osteoblast-like cells on a groove width of (a) 500 nm (153 nm) deposited CaP in an aligned fashion at the interface between cells and the substrate. Aligned CaP deposition at the interface was also observed at a groove width of (b) 50 nm (17 nm depth).



**Fig. 7.** Influence of surface topography on gene expression. (a) Effects of the groove dimensions on gene expression of ALP, OCN, BSP, Col-I, Cbfa1 and the Int α-1 and β-1 by osteoblast-like cells relative to the smooth substrate. Data are expressed as $2^{-\Delta\Delta Ct}$ and range, $n = 3$. Values were normalized to β-actin and relative to smooth substrates. Asterisks: significant difference ($p < 0.05$). (b) Cumulative ranking of osteoblast-specific genes (ALP, OCN, BSP, Col-I and Cbfa1) expressed at three time points (day 1, 3 and 6). The difference in expression of each gene between the four substrates was ranked 1 (lowest expression) to 4 (highest expression) for each time point. The column heights represent the osteoblast-specific gene expression relative to the other groove dimensions.

first assessed by performing an alignment analysis. The current study shows that osteoblasts are responsive to grooves with a nanoscale in all dimensions (groove and ridge width and depth). Zhu et al. [21] and more recently, Yang et al. [20] reported that bone cells aligned to nanogrooves down to respectively 150 nm width and 70 nm in depth or 90 nm width and 300 nm in depth. However, in both studies the actual groove spacing or depth were sub-micrometer and thus not very representative of the natural bone ECM [6]. In the current study, grooved substrates were used which in all dimensions were nanometric, including substrates in the range of natural bone ECM (75 nm groove width and 33 nm depth), to determine the response of osteoblasts in terms of alignment and morphology. Osteoblast response to nanopatterns was first screened using the biochip. From the results of this study, interesting groove dimensions were determined and nanogrooved substrates with a large area were created using laser interference lithography (LIL) and subsequent reactive ion etching (RIE). The major advantage of LIL over other techniques like electron beam lithography and ion beam lithography is the high patterning speed and significantly greater area [29,34]. This step is necessary as only upscaling of production techniques will enable the production of actual orthopedic and dental implants, and later *in vivo* validation of the current experimental results.
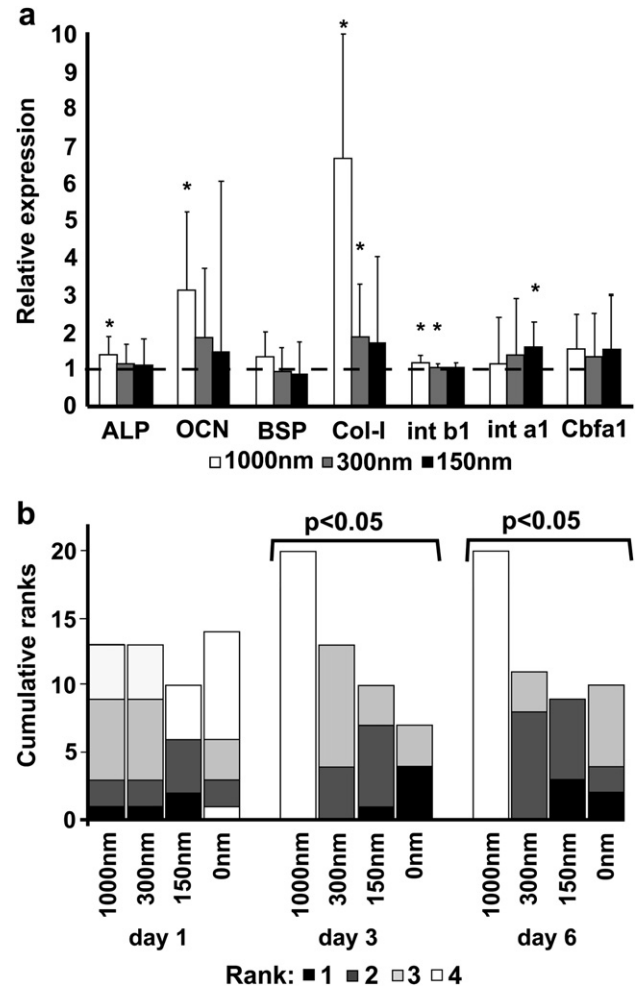
The results from investigations on the cell and cell-substrate interface demonstrate that osteoblast-like cells align to grooves approximating the natural extracellular bone matrix. In this context, focal adhesions are important for the specific recognition and response to the patterns as already described for micrometer ridges [35]. Focal adhesions are associated with the tips of actin filaments, serve to adhere the cell to the ECM proteins and are able to sense the surrounding of the cell [36]. As early as 1979, Ohara and Buck [37] hypothesized that cells cannot align to surface features if focal adhesions cannot sense grooves with an excessive pitch (which is the sum of groove width and ridge width). The results presented in the current study demonstrated that both focal adhesion and cellular alignment decreased similarly with a decreasing groove pitch. Corroborating with the Ohara and Buck theory, these findings implicate that cells cannot align to grooves with a too small pitch because the patterns are not recognized by their focal adhesions.

Scanning and transmission EM studies demonstrated that the ECM mineral CaP is deposited in between the grooves by

osteoblasts in an aligned fashion. This finding corroborates with the *in vivo* situation, where hydroxyapatite crystals deposited by osteoblasts are embedded in the spaces between highly organized collagen-I fibrils of similar dimensions as the grooves [6]. Possibly the osteoblasts recognize the nanogrooved substrate as a natural ECM environment and respond accordingly by the production of an organized ECM. Accordingly, a standardized nano-structured implant surface topography can be important for the formation of an organized bone ECM with high strength starting at the interface between the implant surface and bone tissue. *In vivo* studies are needed to validate whether indeed such an organized extracellular bone matrix is formed.

Alternatively, nanogrooved substrates can serve as a model system *in vitro* for obtaining a better fundamental insight into the initial osteoblasts response to the natural ECM. Recently, Pouget et al. [4] demonstrated that calcium carbonate crystals with a critical size of 70 nm are formed under the control of a negatively charged template. In accordance with this study, nanogrooves might serve as a template (nucleation points) to study structured calcium phosphate mineralization. TEM observations in the current study demonstrated that the amount of CaP deposited by the osteoblasts in between the grooves is increasing. However, the nucleation state of these CaP particles at these and later time points still has to be determined.

Further, the results demonstrated that osteoblast gene expression was highly influenced by individual rat differences. Several studies already demonstrated the advantageous influence of aspecific surface nano-roughness on osteoblast-like gene expression.[38–41] The rank analysis on the gene expression confirmed that a statistically significant upregulation also exists for the ordered nanotextures. Grooved surfaces, and in particular 500 nm wide grooves, are advantageous for osteoblast differentiation. Ponader et al. [39] and Yang et al. [41] demonstrated that gene expression on rough substrates relative to polished controls decreased from day three to seven during incubation. In agreement with these studies, the nanogrooved substrates seem to be specifically effective in the very first days of osteoblast-specific gene expression, which suggests that nanotextures can steer initial osteoblast differentiation.

## 5. Conclusion

In summary, this study proved by using several microscopic techniques and single cell Q-PCR that nanogrooves have a profound influence on osteoblast behavior. Osteoblasts are responsive to nanopatterns down to 75 nm in width and 33 nm in depth. Nano-texture-driven mineral deposition is induced and responsive to even smaller nanopatterns of 50 nm in width and 17 nm in depth. In addition, gene expression of osteoblast specific markers (ALP, OCN, BSP, ColI and Cbfa1) is upregulated by nanogrooves. The results indicate that nanogrooves can be a very promising tool to direct the bone response at the interface between an implant and the bone tissue, which can benefit the installation of implants in compromised patients.

## Acknowledgements

## Appendix. Supplementary material

Supplementary data associated with this article can be found in the online version, at doi:10.1016/j.biomaterials.2010.01.034.

## Appendix

Figures with essential colour discrimination. Certain figures in this article, in particular Figs. 1–4, have parts that are difficult to interpret in black and white. The full colour images can be found in the online version at doi:10.1016/j.biomaterials.2010.01.034.

## References

[1] Stevens MM, George JH. Exploring and engineering the cell surface interface. Science 2005;310(5751):1135–8.
[2] Kasemo B, Gold J. Implant surfaces and interface processes. Adv Dent Res 1999;13:8–20.
[3] Curtis A, Wilkinson C. Topographical control of cells. Biomaterials 1997;18(24):1573–83.
[4] Pouget EM, Bomans PH, Goos JA, Frederik PM, de WG, Sommerdijk NA. The initial stages of template-controlled CaCO3 formation revealed by cryo-TEM. Science 2009;323(5920):1455–8.
[5] Blokhuis TJ, Termaat MF, den Boer FC, Patka P, Bakker FC, Haarman HJ. Properties of calcium phosphate ceramics in relation to their in vivo behavior. J Trauma 2000;48(1):179–86.
[6] Weiner S, Wagner HD. The material bone: structure mechanical function relations. Ann Rev Mat Sci 1998;28:271–98.
[7] Palin E, Liu HN, Webster TJ. Mimicking the nanofeatures of bone increases bone-forming cell adhesion and proliferation. Nanotechnology 2005;16(9):1828–35.
[8] Anderson JM. Inflammation, wound healing, and the foreign-body response. In: Ratner B, Hoffman A, Schoen F, Lemons J, editors. Biomaterial science: an introduction to materials in medicine. San Diego: Elsevier Academic Press; 2004. p. 296–304.
[9] Dalby MJ, McCloy D, Robertson M, Agheli H, Sutherland D, Affrossman S, et al. Osteoprogenitor response to semi-ordered and random nanotopographies. Biomaterials 2006;27(15):2980–7.
[10] Dalby MJ, McCloy D, Robertson M, Wilkinson CD, Oreffo RO. Osteoprogenitor response to defined topographies with nanoscale depths. Biomaterials 2006;27(8):1306–15.
[11] de Oliveira PT, Nanci A. Nanotexturing of titanium-based surfaces upregulates expression of bone sialoprotein and osteopontin by cultured osteogenic cells. Biomaterials 2004;25(3):403–13.
[12] de Oliveira PT, Zalzal SF, Beloti MM, Rosa AL, Nanci A. Enhancement of in vitro osteogenesis on titanium by chemically produced nanotopography. J Biomed Mater Res A 2007;80(3):554–64.
[13] Hansen JC, Yul LJ, Xu LC, Siedlecki CA, Mauger DT, Donahue HJ. Effect of surface nanoscale topography on elastic modulus of individual osteoblastic cells as determined by atomic force microscopy. J Biomech 2007;40(13):2865–71.
[14] Lim JY, Hansen JC, Siedlecki CA, Hengstebeck RW, Cheng J, Winograd N, et al. Osteoblast adhesion on poly(L-lactic acid)/polystyrene demixed thin film blends: effect of nanotopography, surface chemistry, and wettability. Biomacromolecules 2005;6(6):3319–27.
[15] Wan Y, Wang Y, Liu Z, Qu X, Han B, Bei J, et al. Adhesion and proliferation of OCT-1 osteoblast-like cells on micro- and nano-scale topography structured poly(L-lactide). Biomaterials 2005;26(21):4453–9.
[16] Webster TJ, Ergun C, Doremus RH, Siegel RW, Bizios R. Enhanced functions of osteoblasts on nanophase ceramics. Biomaterials 2000;21(17):1803–10.
[17] Webster TJ, Smith TA. Increased osteoblast function on PLGA composites containing nanophase titania. J Biomed Mater Res A 2005;74(4):677–86.
[18] Zhu X, Chen J, Scheideler L, Reichl R, Geis-Gerstorfer J. Effects of topography and composition of titanium surface oxides on osteoblast responses. Biomaterials 2004;25(18):4087–103.
[19] Lenhert S, Meier MB, Meyer U, Chi LF, Wiesmann HP. Osteoblast alignment, elongation and migration on grooved polystyrene surfaces patterned by Langmuir–Blodgett lithography. Biomaterials 2005;26(5):563–70.
[20] Yang JY, Ting YC, Lai JY, Liu HL, Fang HW, Tsai WB. Quantitative analysis of osteoblast-like cells (MG63) morphology on nanogrooved substrata with various groove and ridge dimensions. J Biomed Mater Res A 2008.
[21] Zhu B, Lu Q, Yin J, Hu J, Wang Z. Alignment of osteoblast-like cells and cell-produced collagen matrix induced by nanogrooves. Tissue Eng 2005;11(5, 6):825–34.
[22] Matsuzaka K, Walboomers XF, de Ruijter JE, Jansen JA. The effect of poly-L-lactic acid with parallel surface micro groove on osteoblast-like cells in vitro. Biomaterials 1999;20(14):1293–301.
[23] Teixeira AI, Abrams GA, Bertics PJ, Murphy CJ, Nealey PF. Epithelial contact guidance on well-defined micro- and nanostructured substrates. J Cell Sci 2003;116(Pt 10):1881–92.

[24] Teixeira AI, McKie GA, Foley JD, Bertics PJ, Nealey PF, Murphy CJ. The effect of environmental factors on the response of human corneal epithelial cells to nanoscale substrate topography. Biomaterials 2006;27(21):3945–54.

[25] Loesberg WA, te Riet J, van Delft FCMJM, Schön P, Figdor CG, Speller S, et al. The threshold at which substrate nanogroove dimensions may influence fibroblast alignment and adhesion. Biomaterials 2007;28(27):3944–51.

[26] van Delft FCMJM, Weterings JP, van Langen-Suurling AK, Romijn H. Hydrogen silsesquioxane/novolak bilayer resist for high aspect ratio nanoscale electron-beam lithography. J Vac Sci Technol, B 2000;18(6):3419–23.

[27] van Delft FCMJM, van den Heuvel FC, Loesberg WA, te Riet J, Schön P, Figdor CG, et al. Manufacturing substrate nano-grooves for studying cell alignment and adhesion. Microelectron Eng 2008;85(5, 6):1362–6.

[28] Walboomers XF, Croes HJ, Ginsel LA, Jansen JA. Growth behavior of fibroblasts on microgrooved polystyrene. Biomaterials 1998;19(20):1861–8.

[29] van Soest FJ, van Wolferen HAGM, Hoekstra HJWM, de Ridder RM, Worhoff K, Lambeck PV. Laser interference lithography with highly accurate interfero-metric alignment. Jpn J Appl Phys, Part 1 2005;44(9A):6568–70.

[30] Luttge R, van Wolferen HAGM, Abelmann L. Laser interferometric nanolithography using a new positive chemical amplified resist. J Vac Sci Technol, B 2007;25(6):2476–80.

[31] Maniatopoulos C, Sodek J, Melcher AH. Bone formation in vitro by stromal cells obtained from bone marrow of young adult rats. Cell Tissue Res 1988;254(2):317–30.

[32] Shieh AC, Athanasiou KA. Dynamic compression of single cells. Osteoarthritis Cartilage 2007;15(3):328–34.

[33] Livak KJ, Schmittgen TD. Analysis of relative gene expression data using real-time quantitative PCR and the 2(-Delta Delta C(T)) method. Methods 2001;25(4):402–8.

[34] Curtis AS, Casey B, Gallagher JO, Pasqui D, Wood MA, Wilkinson CD. Substratum nanotopography and the adhesion of biological cells. Are symmetry or regularity of nanotopography important? Biophys Chem 2001; 94(3):275–83.

[35] den Braber ET, Jansen HV, de Boer MJ, Croes HJ, Elwenspoek M, Ginsel LA, et al. Scanning electron microscopic, transmission electron microscopic, and confocal laser scanning microscopic observation of fibroblasts cultured on microgrooved surfaces of bulk titanium substrata. J Biomed Mater Res 1998;40(3):425–33.

[36] Wozniak MA, Modzelewska K, Kwong L, Keely PJ. Focal adhesion regulation of cell behavior. Biochim Biophys Acta 2004;1692(2, 3):103–19.

[37] Ohara PT, Buck RC. Contact guidance in vitro. A light, transmission, and scanning electron microscopic study. Exp Cell Res 1979;121(2):235–49.

[38] Kubo K, Att W, Yamada M, Ohmi K, Tsukimura N, Suzuki T, et al. Microtopography of titanium suppresses osteoblastic differentiation but enhances chondroblastic differentiation of rat femoral periosteum-derived cells. J Biomed Mater Res A 2008.

[39] Ponader S, Vairaktaris E, Heinl P, Wilmowsky CV, Rottmair A, Korner C, et al. Effects of topographical surface modifications of electron beam melted Ti-6Al-4V titanium on human fetal osteoblasts. J Biomed Mater Res A 2008; 84(4):1111–9.

[40] Tsai SW, Chen CC, Chen PL, Hsu FY. Influence of topography of nanofibrils of three-dimensional collagen gel beads on the phenotype, proliferation, and maturation of osteoblasts. J Biomed Mater Res A 2008.

[41] Yang XF, Chen Y, Yang F, He FM, Zhao SF. Enhanced initial adhesion of osteoblast-like cells on an anatase-structured titania surface formed by $H_2O_2$/HCl solution and heat treatment. Dent Mater 2009;25(4): 473–80.